Applied Catalysis B: Environmental 166–167 (2015) 518–528

Contents lists available at ScienceDirect

Applied Catalysis B: Environmental

journal homepage: www.elsevier.com/locate/apcatb

Highly active Au-CeO_2@ZrO_2 yolk–shell nanoreactors for the reduction of 4-nitrophenol to 4-aminophenol

Viridiana Evangelista [a], Brenda Acosta [a], Serguei Miridonov [b], Elena Smolentseva [c], Sergio Fuentes [c], Andrey Simakov [c,*]

[a] Posgrado en Física de Materiales, Centro de Investigación Científica y de Educación Superior de Ensenada, Carretera Ensenada-Tijuana 3918, Zona Playitas, C.P. 22860 Ensenada, Baja California, Mexico
[b] Departamento de Óptica, Centro de Investigación Científica y de Educación Superior de Ensenada, Carretera Ensenada-Tijuana 3918, Zona Playitas, C.P. 22860 Ensenada, Baja California, Mexico
[c] Universidad Nacional Autónoma de México, Centro de Nanociencias y Nanotecnología, Km. 107 Carretera Tijuana a Ensenada, C.P. 22860 Ensenada, Baja California, Mexico

ARTICLE INFO

Article history:
Received 9 July 2014
Received in revised form
21 November 2014
Accepted 2 December 2014
Available online 4 December 2014

Keywords:
Ceria
Decoration
Gold
Nanoreactors
4-Nitrophenol reduction

ABSTRACT

Highly catalytically active yolk–shell Au-CeO_2@ZrO_2 nanoreactors (gold core encapsulated into porous zirconia shell and doped by ceria) for the 4-nitrophenol reduction to 4-aminophenol were synthesized. Au cores encapsulated into SiO_2 (Au@SiO_2) were decorated with ceria via injection of ceria precursor into a void space of silica shell (formed through surface-protected etching of silica by hot water) with its subsequent hydrolysis and thermal treatment (Au-CeO_2@SiO_2). Au-CeO_2@ZrO_2 nanoreactors were obtained using Au-CeO_2@SiO_2 as a template and replacement of SiO_2 by ZrO_2. The nanoreactors were characterized by STEM-EDS, in situ and ex situ UV–vis spectroscopy, and N_2 thermal adsorption. The catalytic activity for decorated Au-CeO_2@ZrO_2 nanoreactors in the 4-nitrophenol reduction into 4-aminophenol was found to be ~3 times higher than for non-decorated Au@ZrO_2 nanoreactors. The herein proposed route of nanoreactor core decoration may be applied for the synthesis of nanoreactors with cores modified with different materials in order to make them effective for different catalytic reactions.

1. Introduction

Gold nanoparticles (Au NPs) have a great potential in many reactions important for environmental protection, such as reduction of nitro-aromatic compounds, CO oxidation, water-gas shift reaction, etc. [1–7]. However, they easily aggregate due to their high surface energy, resulting in changes in the size and shape of the NPs during the catalytic reaction with the consequent decay in their catalytic activity [8–11]. Existing strategies for Au NPs stabilization can be roughly divided into two categories: physical and chemical. In the physical approach the NPs are separated from each other by a physical barrier so that they cannot contact each other directly: (i) colloidal NPs stabilized by electrostatic forces or steric stabilizers [12–14]; (ii) NPs located inside of the channels of relatively inert materials such as mesoporous silica [15] or zeolites [16,17]; and (iii) NPs encapsulated into porous spheres [18,19]. Chemical approaches are based on substrate effects or on the formation of alloy or hybrid materials: (i) NPs supported on chemically active oxides (e.g. titania [20] or ceria [21]); (ii) bimetallic NPs (e.g. Au–Ag alloy [22]). Among techniques listed above the application of core–shell and yolk–shell materials with gold nanoparticle cores and porous shells is a fruitful way to prevent sintering of Au NPs [23,24].

Yolk–shell materials (nanoreactors) represent a new generation of heterogeneous catalysts with excellent catalytic stability due to their specific structure, which consists of a core, commonly the active phase, surrounded by a porous shell in a core@void@shell arrangement [25–30]. Compared with conventional catalysts supported on bulk supports, each nanoparticle in the yolk–shell nanoreactor is isolated by a highly porous shell and has a relatively homogeneous surrounding environment. Their properties (structure stability, catalytic stability as well as mass transfer of reactants and products, etc.) have been investigated in detail. It was shown that nanoreactors are thermally very stable, which maintains the integrity of the system; without substantial mass transfer resistance; and preserve catalytic activity after high-temperature treatments [26,27,31–35]. There are two general routes for the yolk–shell nanoreactor preparation: top-down and bottom-up

* Corresponding author. Tel.: +52 646 175 06 50x353; fax: +52 646 174 46 03.
E-mail address: andrey@cnyn.unam.mx (A. Simakov).

http://dx.doi.org/10.1016/j.apcatb.2014.12.006
0926-3373/

[36,37]. For the preparation of Au@ZrO_2 (gold core encapsulated into porous zirconia shell) nanoreactor, the bottom-up route commonly consists of: (1) Au core formation; (2) covering of the Au core with silica; (3) covering with the ZrO_2 precursor; (4) calcination of the sample in order to form a ZrO_2 shell, and (5) leaching of SiO_2 via sample treatment with a concentrated base, which gives rise to the formation of the yolk–shell structure with a free-moving Au core inside the ZrO_2 porous shell [19,38,42].

According to the commonly reported diameter of oxide shell pores (2.5–5 nm), the size of the metal core should be above 5 nm in order to prevent its free release from the porous shell. A significant decrease in pore size causes diffusion problems. Thus, there is a balance between pore size and mass transfer resistance [25,30,34,35,39]. On the other hand, the catalytic activity of Au NPs depends on their size [1,4,8]. As an example, significant difference in CO oxidation was found for Au NPs with size within the 1–5 nm range [40,41], while activity for large Au NPs with size between 5 and 15 nm was similar [42].

Thus, for some reactions, where the size of the participating molecules is small enough (e.g. CO oxidation), highly active nanoreactors may be designed with small gold cores and shells that have small pores [43,44]. Other way to enhance the catalytic performance of nanoreactors with relatively large pores and cores is decoration/doping of their cores, which became relevant for the reactions including relatively large molecules [45,46]. Recently, it was found that the decoration of silica-supported Au NPs with CeO_2 increases CO oxidation activity [47]. Even the decoration of the catalytically inert Au film with CeO_2 nanoparticles resulted in the enhancement of CO oxidation activity by three orders of magnitude [48]. Thus, the catalytic activity of relatively large Au NPs may be improved via covering or decorating them with cerium or titanium oxides; this promotes the formation of new highly active sites on the Au-oxide interface [49,50].

A positive effect of the gold-ceria interface on CO oxidation was reported for gold based nanoreactors [51,52] and 4-nitrophenol reduction for yolk–shell Au/CeO_2@CeO_2 (numerous gold NPs being supported on the external surface of ceria sphere are covered with the second porous ceria shell) and @Au/CeO_2 (relatively small gold NPs are supported on the internal surface of the hollow ceria sphere) nanoreactors [53,54]. In addition, the ceria nanorods containing a {1 1 0} plane were found to catalyze the reduction of nitroaromatics, while nanoceria with a {1 0 0} or {1 1 1} planes shows poor performance in this reaction [55]. Deposition of Au NPs on ceria nanotubes or ceria spheres resulted in the appearance of Au cations and a drastic enhancement of 4-nitrophenol reduction [56]. It was experimentally found that the high efficiency of ceria to adsorb nitro aromatic molecules leads to the appearance of a second route of nitro aromatics reduction over Au NPs supported on ceria via the condensation of some intermediates with the resulting formation of amino products [57,58].

Herein, we propose to enhance catalytic performance of Au@SiO_2 and Au@ZrO_2 yolk–shell nanoreactors well presented in the literature via decoration of their Au cores with ceria.

2. Experimental

2.1. Synthesis of non-decorated nanoreactors

The non-decorated nanoreactors were synthesized following the conventional bottom-up route [23] presented in Fig. 1. All reactants were used without further purification.

2.1.1. Au@SiO_2 nanoreactors

Colloidal Au NPs with a mean particle size of 15 ± 5 nm (according to TEM analysis presented in Fig. S1 (Supplementary data)) were prepared in a reflux system with vigorous stirring as in Ref. [23,59,60]. First, deionized water (125 mL) was mixed with $HAuCl_4$ (Alfa-Aesar) solution (25 mL, 2.54 mM) and heated until boiling point. Then $C_6H_5O_7Na_3$ (Sigma Aldrich) solution (12.5 mL, 0.39 M) was added. After 30 min, the obtained gold colloid was cooled to room temperature and mixed with a freshly prepared polyvinylpyrrolidone (PVP-10, Sigma Aldrich) solution (0.325 mL, 12.8 mg/mL) for 5 days.

Gold NPs were encapsulated into silica shells by the Stöber method [61,62]. Briefly, the gold NPs stabilized by PVP were separated by centrifugation and, after the volume was adjusted to 6 mL with deionized water, they were ultrasonically dispersed. Then absolute ethanol (18.90 mL, Jalmek) premixed with a concentrated ammonia solution (0.84 mL, Sigma Aldrich) was added under vigorous magnetic stirring. Immediately afterwards, a solution of TEOS (1.19 mL, Sigma Aldrich) in absolute ethanol (12.80 mL, Jalmek) was added dropwise under vigorous stirring at room temperature overnight. Thereafter, the solution was centrifuged, and the separated solid powder containing the silica-encapsulated Au NPs was washed several times with water.

Finally, a surface-protected etching process with hot water was used to enhance the porosity of the silica shell as in [24,63–65]. A PVP-10 solution (0.325 mL, 12.8 mg/mL) was added under vigorous magnetic stirring to the freshly prepared silica-encapsulated Au NPs dispersed in water. Then the mixture was heated to boiling point for 7 h under reflux, cooled to room temperature and centrifuged. The obtained solid sample was washed several times with water and dried at 120 °C for 2 h. Finally, Au@SiO_2 (Au 9.6 wt.%) nanoreactors were thermally treated at 450 °C in N_2 flow and then at 750 °C in O_2 flow with a ramp rate of 2 °C/min for decomposition of residual organic compounds. Evolution of the shell structure due to the etching process was revised by TEM (Fig. 2, Fig. S2 in the Supplementary data). Etching resulted in the changes of silica shell contrast in TEM image (compare Fig. 2A and B). In addition, some light zones around the Au cores appeared (marked by white arrow in Fig. 2B). These light zones were assigned to the void space in the silica matrix. It was concluded that the silica spheres were reconstructed after etching and thermal treatment by the condensation of silica species with consequent formation of the void space close to the Au cores. Enhancement of silica shell porosity was confirmed by nitrogen adsorption measurements (Fig. 2). Etching resulted in the appearance of pores with the size around 40 nm, which is comparable with dimensions of the light zones found in TEM images.

2.1.2. Au@ZrO_2 nanoreactors

The fresh silica-encapsulated Au NPs were washed several times in pure ethanol and redispersed at 30 °C in a mixture of pure ethanol (31.7 mL) and aqueous solution of pentaethylene glycol monododecyl ether (0.15 mL, 96 mM, Sigma). After vigorous stirring for 1 h, zirconium butoxide (0.45 mL, Aldrich) was added and the formed solution was stirred overnight. The solid sample obtained by centrifugation was washed with deionized water four times and aged in water at room temperature for 3 days. Then the sample was dried at 110 °C for 1 day and treated at 450 °C in N_2 flow and at 900 °C in O_2 flow with a ramp rate of 2 °C/min to form Au@SiO_2@ZrO_2.

Finally, the silica was removed via treatment of the obtained Au@SiO_2@ZrO_2 sample with concentrated NaOH solution. First, the sample was kept in NaOH (1 M, Jalmek) at room temperature under constant magnetic stirring for 16 h. Subsequently, the alkaline solution was exchanged by a fresh one and the procedure continued for an additional 12 h at 50 °C. The obtained yolk–shell Au@ZrO_2 (Au 0.05 wt.%) nanoreactors were washed five times with water and once with ethyl tert-butyl ether (Sigma Aldrich). According to the statistical analysis of TEM images of prepared Au@ZrO_2 nanoreactors the average diameter and thickness of the zirconia shell were

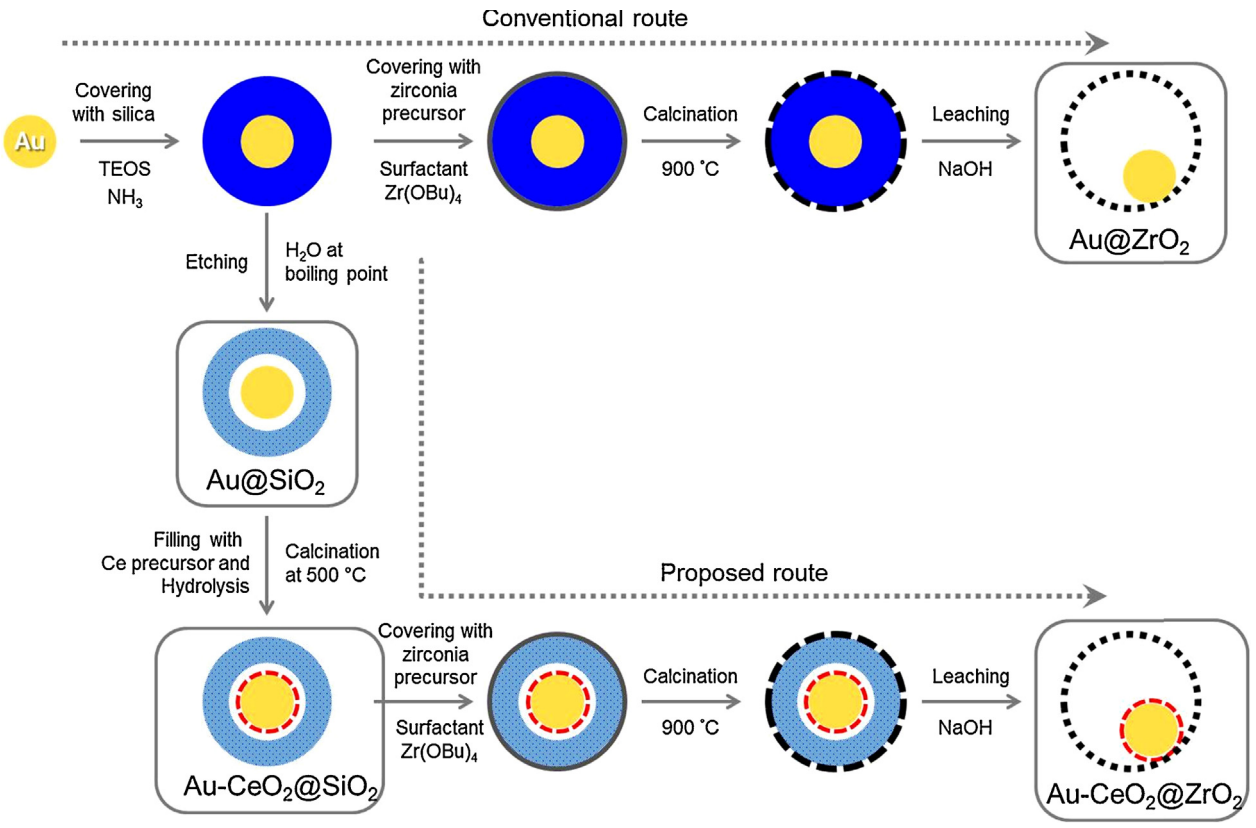

Fig. 1. General scheme for $Au@SiO_2$, $Au@ZrO_2$, $Au\text{-}CeO_2@SiO_2$ and $Au\text{-}CeO_2@ZrO_2$ nanoreactors synthesis.

equal to 110 ± 18 nm and 11 ± 2.5 nm, respectively (see Supplementary data Figs. S3 and S4).

2.2. Sample characterization

2.2.1. Transmission electron microscopy

The structure of the yolk–shell nanoreactors and the distribution of elements were determined by STEM using a JEOL JEM-2100F microscope with an XMAX OXFORD detector. EDX analysis for the selected elements was carried out using the INCA software. For the EDS analysis, the used probe size was 1.7 nm with a current of 130 mA. Prior to analysis, the samples were dispersed in propan-2-ol and dropped on a copper grid coated with carbon film. To determine the mean diameter of cores and shells, and shell thickness, more than 100 specimens were measured.

2.2.2. N_2 adsorption

The porous structure of prepared samples was determined using BET method, by nitrogen adsorption measurements in a Micromeritics TriStar II-3020 device. Before analysis, samples were

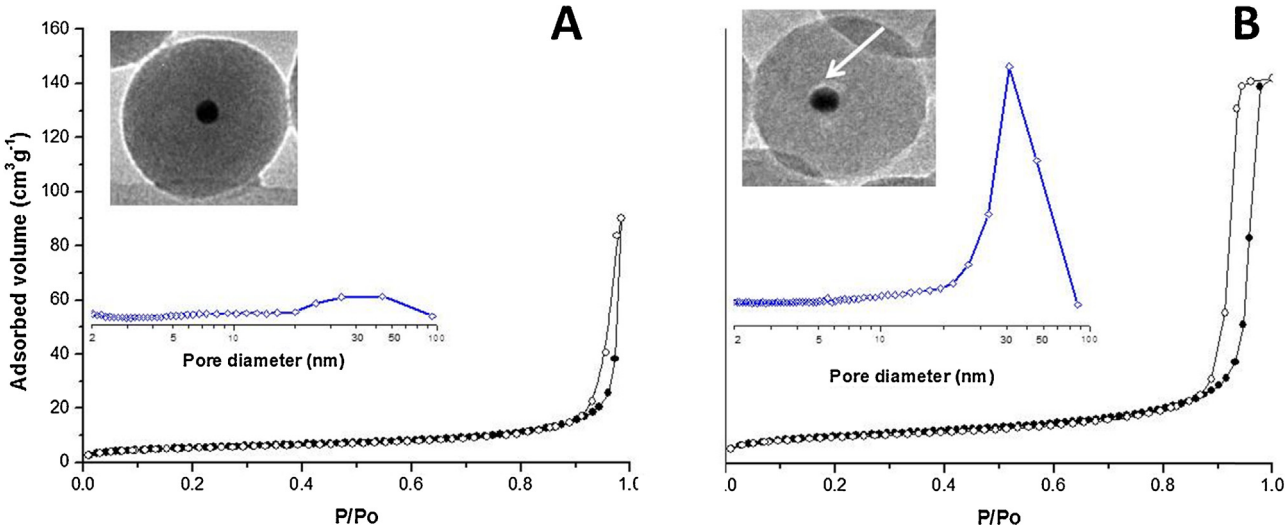

Fig. 2. N_2 adsorption–desorption isotherms for $Au@SiO_2$ samples before (A) and after (B) the etching process. Insets present the pore size distribution curves and a corresponding typical TEM image.

treated in vacuum (10^{-3} Torr) at 200 °C for 4 h using a Micromeritics VacPrep 061-Sample degas system.

2.2.3. UV–vis spectroscopy

The prepared samples were studied by UV–vis spectroscopy. Spectra were recorded using an AVANTES Ava-Spec-2048 UV–vis spectrometer equipped with an AvaLight-DHS light source. Ex situ spectra were measured at room temperature. In situ UV–vis measurements at high temperature were carried out in a lab-made set-up. In this case, the high temperature optic fiber reflection probe was located close to the external wall of the quartz reactor. UV–vis spectra recorded each 15 s (time of spectrum recording was about 5 ms) were obtained by subtraction of the initial spectrum recorded at room temperature from those recorded at elevated temperatures. MgO was used as a reference.

2.2.4. Reduction of 4- and 2-nitrophenols

The obtained nanoreactors were tested in the 4- and 2-nitrophenol reduction with excess $NaBH_4$ as reducing agent at room temperature. The aqueous suspension of nanoreactors (1.4 mg/mL) was ultrasonically treated for 30 min before the catalytic run. In a typical experiment, freshly prepared 0.3 mL of nitrophenol (1 mM) and 3.7 mL of $NaBH_4$ (1 mM) aqueous solutions were mixed in a quartz cuvette (1 cm of optical path, volume 4 mL) for 15 min. Then 0.1 mL of nanoreactor suspension was injected by micropipette under constant magnetic stirring of the reaction mixture. Reaction progress was monitored on-line by UV–vis spectroscopy in transmittance mode using the same spectrometer as described above. The spectra were collected every 60 s until the complete consumption of nitrophenol (monitoring disappearance of peak at 400 nm). Experiments were repeated 3 times to confirm the activity level reproducibility. Reactants of analytic grade (Sigma–Aldrich) were used for the activity test.

2.2.5. CO oxidation

Catalytic activity in CO oxidation for the prepared nanoreactors was measured at atmospheric pressure in a U-Shape quartz flow reactor (i.d. 4 mm, o.d. 6 mm). Prior to the catalytic run, samples (0.03 g) were pre-treated in oxygen flow with a temperature increase up to 350 °C using a ramp rate of 5 °C/min and then purged with nitrogen until the temperature decreased to 25 °C. The reactant gas mixture consisted of 1 vol.% CO and 0.5 vol.% O_2 in nitrogen with total flow rate of 80 mL/min. Catalytic runs were performed with a temperature increase within the 25–500 °C interval and a ramp rate of 2 °C/min. Reactants and products were analyzed using a CAI ZRE gas analyzer. Catalyst temperature was measured by a thin thermocouple with a fast response placed inside the reactor in contact with the catalyst bed. Catalytic activity of the samples was characterized by values of CO conversion vs temperature. Gases of high purity grade were used in the catalytic experiments without further purification.

3. Results and discussion

3.1. Decoration of gold cores in nanoreactors

In order to modify the properties of the gold cores in the nanoreactors we propose decoration of them with ceria (see Fig. 1). According to the scheme, the void space of the Au@SiO_2 nanoreactors formed by the etching process was first filled with an aqueous solution of ceria precursor and urea at room temperature applying the commonly used approach in the top-down route of nanoreactors preparation when previously formed hollow spheres are filled with precursors to obtain nanoreactor cores [26,66–68]. Cerium salt was hydrolyzed into cerium hydroxide by thermal treatment of the sample. High efficiency of urea to hydrolyze cerium salt at elevated temperatures is shown in [69]. The formed cerium hydroxide is then transformed into ceria by the calcination. The herein obtained Au-CeO_2@SiO_2 nanoreactor was used as a precursor to prepare the Au-CeO_2@ZrO_2 nanoreactor following the conventional steps described in the experimental section: (i) covering of the silica shell with ZrO_2 precursor; (ii) calcination of the sample in order to form a ZrO_2 shell; and, finally, (iii) leaching of SiO_2 via treatment of the Au@SiO_2@ZrO_2 sample with a base, which leads to the formation of a yolk–shell structure with a free-moving Au core inside the ZrO_2 porous shell.

3.1.1. Au-CeO_2@SiO_2 nanoreactors

To form ceria species in the free space (Fig. 2B, marked by arrow) around the Au cores in the Au@SiO_2 nanoreactor, the free space was filled with an aqueous solution of cerium nitrate (3.5 M) and urea (21 M) via incipient wetness impregnation. Then the sample was heated to 85 °C for 15 h and subsequently to 120 °C for 2 h. The UV–vis spectrum of the Au@SiO_2 sample (Fig. 3A, marked as I) showed a characteristic band centered at 518 nm attributed to the plasmon band of the free Au cores as described in [70]. After hydrolysis of the cerium nitrate, the plasmon band shifted to 640 nm (Fig. 3A, marked as II). This shift may be related to the strong interaction of the Au cores with the formed cerium hydroxide species [71]. We believe that at that point gold NPs were in close contact with cerium hydroxide.

In order to convert cerium hydroxide into ceria, the Au-$Ce(OH)_3$@SiO_2 sample was calcined up to 500 °C with a ramp rate of 2 °C/min in Ar with a total flow rate of 80 mL/min. It is known that $Ce(OH)_3$ dehydrates progressively with formation of CeO_2 under thermal treatment [72]. The formation of ceria and its interaction with the Au core was monitored by means of in situ UV–vis spectroscopy (Fig. 3B). The first detectable changes in the UV–vis spectra were observed at temperatures above 100 °C. With further temperature rise, peaks around 450, 570 and 700 nm appeared and then increased in intensity. The first peak was assigned to the adsorption edge of ceria [21,73], while two further peaks were attributed to the plasmon of Au cores in contact with ceria, and to surface defects of amorphous ceria species, respectively. The attribution of the peak at 700 nm to surface defects was based on the data of the thermal treatment of reference ceria sample in hydrogen or oxygen flow (see Fig. S5, Supplementary data). The peak related to amorphous ceria drastically decreased in intensity at temperatures above 350 °C (marked by arrow in Fig. 3B). At the same temperature, rapid conversion of cerium hydroxide into ceria was observed in the TGA profile [72]. Thus, it may be concluded that the thermal treatment of the Au-$Ce(OH)_3$@SiO_2 sample resulted in the formation of Au-CeO_2@SiO_2 nanoreactors.

The UV–vis spectrum of the obtained Au-CeO_2@SiO_2 nanoreactors (Fig. 3A, marked as III) was characterized by the presence of the Ce-O charge transfer band at 240 nm and the plasmon band of the Au cores at 550 nm. The red shift of the plasmon band for Au-CeO_2@SiO_2 nanoreactor with respect to the band for the Au@SiO_2 nanoreactor indicates that Au cores are still interacting with the formed ceria [74]. Analysis of Ce and Au element distribution across the Au-CeO_2@SiO_2 nanoreactor with the STEM-EDS line-scanning technique confirmed the preferable formation of ceria around the Au core (Fig. 3C), considering that Ce profile intensity shows a maximum in the zone of the Au core.

3.1.2. Au-CeO_2@ZrO_2 nanoreactors

The Au-CeO_2@ZrO_2 nanoreactor was prepared following the steps of the proposed route (illustrated in Fig. 1) and using the Au-CeO_2@SiO_2 nanoreactor as a template. STEM data of the obtained Au-CeO_2@ZrO_2 nanoreactors are presented in Fig. 4. The structure of the obtained Au-CeO_2@ZrO_2 and Au@ZrO_2 nanoreactors was

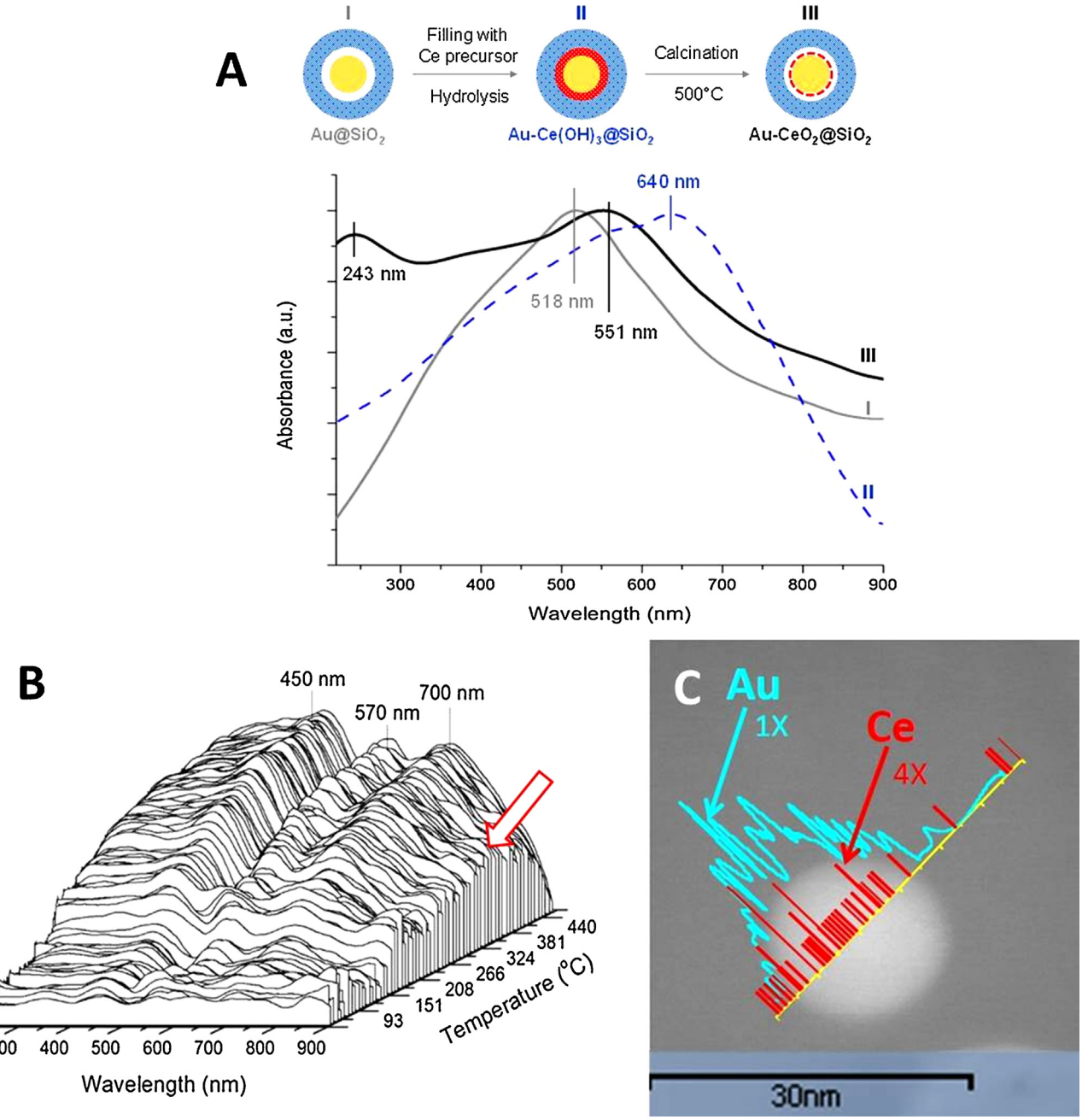

Fig. 3. UV–vis spectra recorded ex situ (A) or in situ (B) during calcination of the Au-CeO_2@SiO_2 sample up to 500 °C. (C) Profiles of Au and Ce distribution across an Au-CeO_2@SiO_2 nanoreactor according to the STEM-EDS line-scanning technique.

practically the same (Fig. 4, Fig. S3 in Supplementary data). Comparing EDX spectra for different zones of Au-CeO_2@ZrO_2 nanoreactor it may conclude that the ceria is distributed now in the whole internal space of nanoreactor. Some portion of ceria was found even close to internal zirconia shell. The size of the void space in Au-CeO_2@ZrO_2 was much larger than that in Au-CeO_2@SiO_2. Elimination of the silica shell during the synthesis of Au-CeO_2@ZrO_2 nanoreactors led to redistribution of the ceria particles. The redistribution of ceria inside the Au-CeO_2@ZrO_2 nanoreactor resulted in a partial decrease of Ce content near the gold core. In turn, the decrease of Ce content around the Au core can affect the number of gold-ceria contact points. This observation agrees with the UV–vis analysis of the obtained nanoreactors. Indeed, the position of the plasmon band in the UV–vis spectra for Au-CeO_2@ZrO_2 and Au@ZrO_2 nanoreactors was practically the same (Fig. 5). Therefore, the effect of ceria on the electronic state of the Au cores is not significant now. However, the presence of ceria in the Au-CeO_2@ZrO_2 nanoreactor was shown by the adsorption in the interval 200–500 nm, typical for the ceria adsorption edge [21] (see Fig. 5, subtraction curve). In addition, residual silica was found in the sample (Fig. 4). A similar effect is described in [50], where a strong interaction of residual silica with the zirconia phase results in the formation of Zr–Si–O, a new compound on the internal surface of the zirconia shell.

3.2. Catalytic activity test

3.2.1. Reduction of the 4- and 2-nitrophenols

The nitro-aromatic compounds commonly produced in the industrial manufacture of agrochemicals, dyes and pharmaceuticals can be reduced into their corresponding useful aromatic

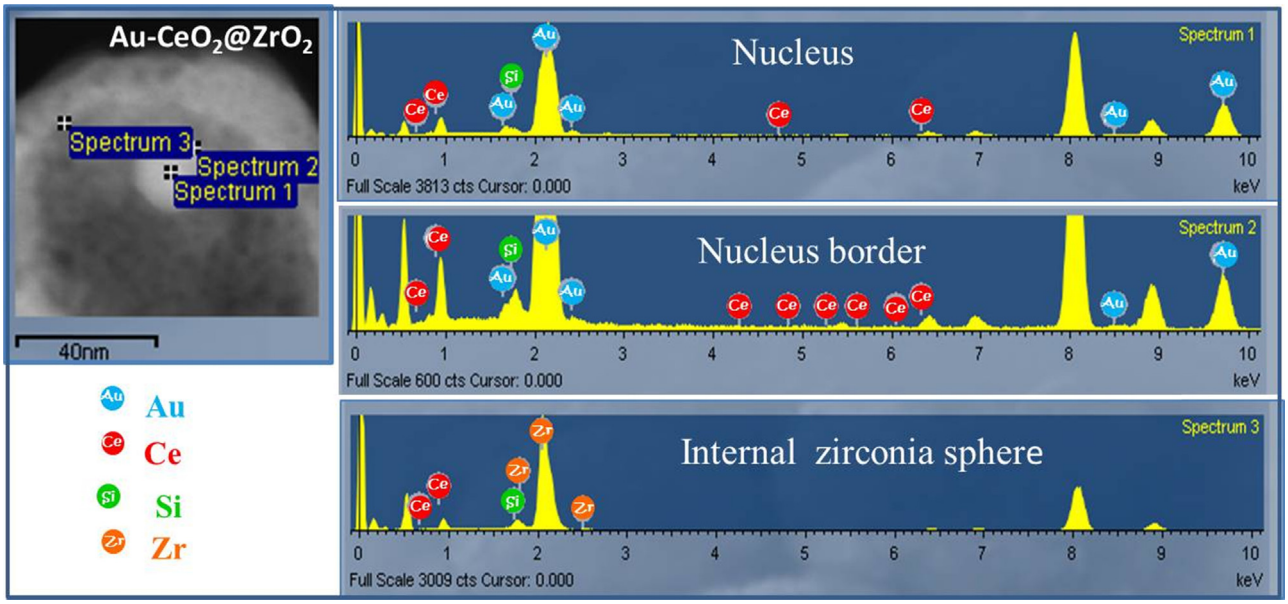

Fig. 4. Typical STEM image of Au-CeO_2@ZrO_2 nanoreactors (left). EDX spectra of Au, Zr, Ce and Si elements in some selected zones of Au-CeO_2@ZrO_2 nanoreactor (right).

amines in the presence of Au NPs [75,76]. Presently obtained nanoreactors were tested in reaction of the 4-nitrophenol reduction to 4-aminophenol with excess $NaBH_4$ as reducing agent at room temperature. Typical evolution of UV–vis spectra collected during the 4-nitrophenol reduction in the presence of Au-CeO_2@ZrO_2 nanoreactors is shown in Fig. 6A. 4-Nitrophenol in contact with $NaBH_4$ was transformed to the corresponding nitrophenolate ion characterized by a strong absorbance peak at 400 nm (see Supplementary data Fig. S6). The characteristic peak for the 4-nitrophenolate ion decreased with time of reaction; while a new peak at 300 nm attributed to 4-aminophenol appeared as in [77–80]. The last spectrum recorded at the end of the reaction coincided well in position with that for the reaction product (4-aminophenol) and its intensity corresponded to the expected final concentration. Commonly, the reaction of nitrophenol reduction by excess $NaBH_4$ is described by a first-order rate law with respect to nitrophenolate ion concentration [80–83]. Thus, the value of the apparent reaction rate constants was estimated from a linear slope of the relative nitrophenolate ion content (A/A_o) in logarithmic form (see Fig. 6B).

The estimated values of the apparent reaction rate constants (0.024 and 0.008 s^{-1}) are represented by bars in Fig. 7 for decorated and non-decorated Au@ZrO_2 nanoreactors. The presence of ceria in close contact with gold cores improved the catalytic activity by approximately 3 times in comparison with that for non-decorated Au@ZrO_2 nanoreactors.

Activity of the synthesized nanoreactors in the 4-nitrophenol reduction to 4-aminophenol was compared with data in the

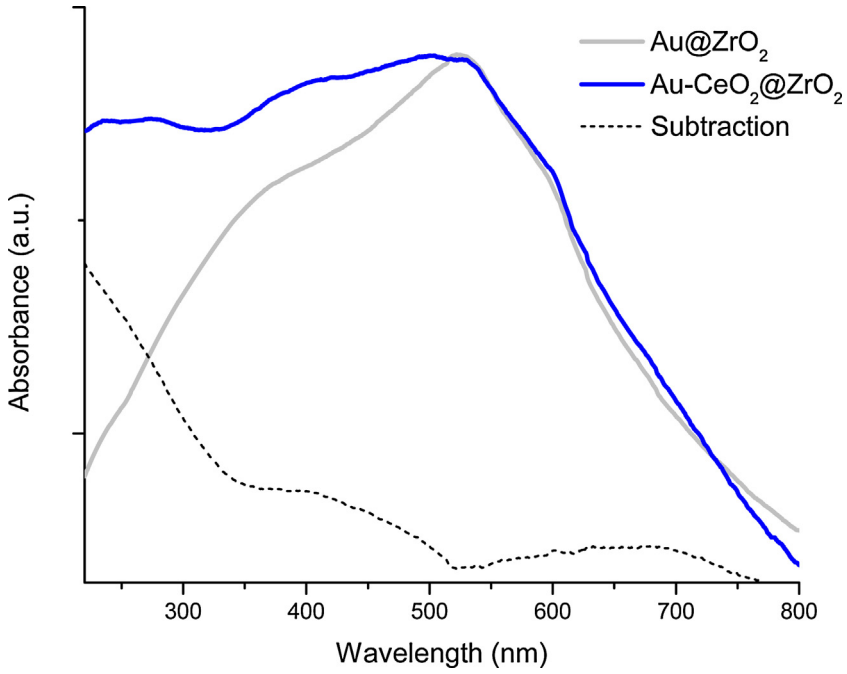

Fig. 5. UV–vis spectra of Au@ZrO_2 and Au-CeO_2@ZrO_2 nanoreactors. Dot line presents the difference between experimental spectra.

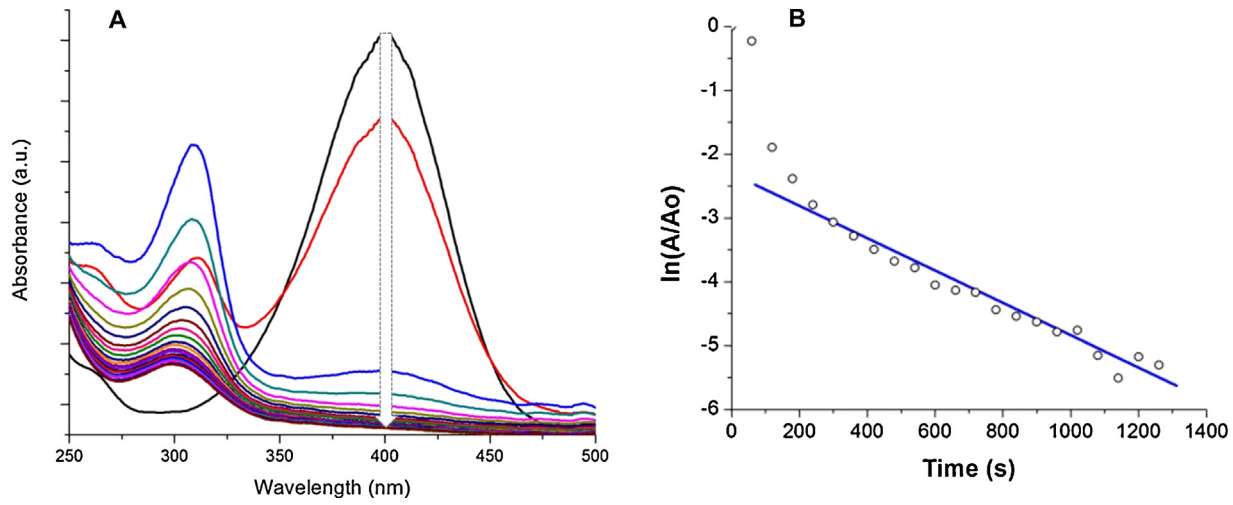

Fig. 6. Catalytic reduction of 4-nitrophenol by excess $NaBH_4$ in the presence of Au-CeO_2@ZrO_2 nanoreactors monitored by in situ UV–vis spectroscopy at room temperature (A). The change in absorbance at 400 nm corresponding to 4-nitrophenolate consumption in logarithmic form vs reaction time (B).

literature for reference nanoreactors and supported catalysts (see Table 1). All catalytic data were obtained at room temperature in the excess of $NaBH_4$. To exclude an effect of the gold content, the values of the estimated apparent rate constant were normalized with respect to gold content (μmol) and gold dispersion to obtain *K* and TOF, respectively. Au dispersion was estimated from the size of gold cores found by TEM, assuming they have spherical shape. The value for *K* for presently prepared Au@ZrO_2 nanoreactors was comparable with that for similar systems [18] (see Table 1). From data presented in Table 1 it may be concluded that two main factors affect the catalytic activity of gold NPs: (i) size and shape of gold NPs and (ii) gold-support interface. Nanoreactors with small Au cores usually show a higher activity in the reduction of 4-nitrophenol than those with large Au cores [30]. However, activity of presently prepared Au@ZrO_2 nanoreactors with relatively large Au cores (15 nm) was higher than Au@ZrO_2 nanoreactors with Au cores of 6 nm reported by Huang [18]. The differences in activity for the Au@ZrO_2 samples of present work and those of Huang may be attributed to the effect of residual silica. Indeed, the presence of residual silica can negatively affect the activity of the nanoreactors via partial blocking either of the gold core or the shell [50]. The highest activity in the reduction of 4-nitrophenol over gold based nanoreactors was observed in the literature for yolk–shell Au/CeO_2@CeO_2 nanoreactors with numerous tiny Au NPs supported on the external surface of the ceria core and then covered by a second porous ceria shell [53]. However, the TOF value for this system is a little lower than that estimated for the presently prepared decorated Au-CeO_2@ZrO_2 nanoreactor.

The enhanced activity of gold-ceria nanoreactors may be explained by electron transfer between ceria and Au NPs, facilitating the uptake of electrons by nitrophenol molecules as in case of Au/graphene [84]. Note that no drastic changes were found in the

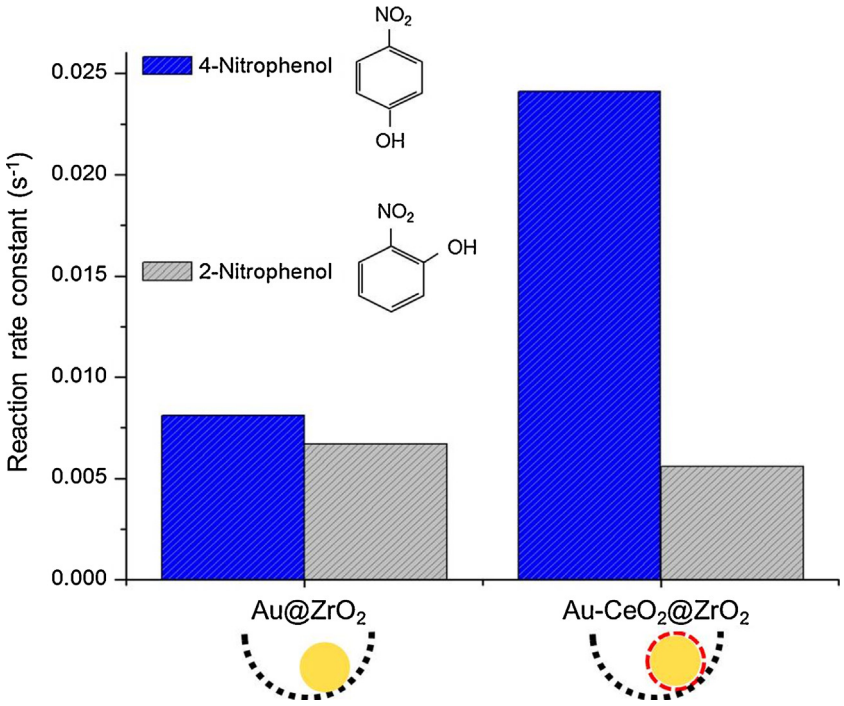

Fig. 7. Apparent reaction rate constants for the reduction of 4-nitrophenol and 2-nitrophenol by $NaBH_4$ in the presence of Au@ZrO_2 and Au-CeO_2@ZrO_2 nanoreactors.

Table 1
Reaction rate constant (K) and TOF for the 4-nitrophenol reduction to 4-aminophenol with an excess $NaBH_4$ at room temperature over different Au-based catalysts.

Catalyst	Core diameter (nm)	Molar ratio Au:4NP	Molar ratio $NaBH_4$:4NP	Au content in reaction mixture (μmol)	k_{app} (s^{-1})	K[a] (s^{-1} μmol Au^{-1})	Au dispersion, parts	TOF[b]	Ref. no.
$Au/CeO_2@CeO_2$[d]	4	607:1	1333:1	91	0.0128	2.822	0.288	9.8	[49]
$AuNPs/CeO_2$-NTs[e]	5		42:1			0.014[c]	0.234	0.1	[52]
$@Au/CeO_2$[f]	3–5		83:1			0.096[c]	0.288	0.3	[50]
$Au@ZrO_2$[g]	6	9:1	176:1	63	0.0052	0.207	0.192	1.1	[18]
$Au@ZrO_2$[g]	15	947:1	1233:1	284	0.0081	0.285	0.077	3.7	This work
$Au\text{-}CeO_2@ZrO_2$[h]	15	947:1	1233:1	284	0.0241	0.848	0.077	11.0	This work

[a] Activity parameter K is the ratio of the apparent rate constant (k_{app}) to the total mass of Au (μmol) added to the reaction media.
[b] TOF = K/Au dispersion. Au dispersion was estimated based on the size of gold cores (found by TEM) using formula: Au dispersion = 8 × radius of Au atom (nm)/gold core diameter (nm).
[c] Values of activity parameter (K) were estimated by authors in cited references.
[d] $Au/CeO_2@CeO_2$ (numerous gold nanoparticles supported on the external surface of ceria core and covered with the second porous ceria shell).
[e] $AuNPs/CeO_2$-NTs (gold nanoparticles supported on the external surface of ceria nanotubes).
[f] $@Au/CeO_2$ (numerous relatively small gold nanoparticles supported on the internal surface of hollow ceria sphere).
[g] $Au@ZrO_2$ (yolk shell structure where single gold nanoparticle is encapsulated into hollow porous zirconia shell).
[h] $Au\text{-}CeO_2@ZrO_2$ (yolk shell structure where single gold nanoparticle and ceria are encapsulated into hollow porous zirconia shell).

Table 2
TOF values for CO oxidation at 140 °C over Au-based nanoreactors and supported catalysts.

Catalyst	Au diameter (nm)	Au content (wt. %)	Flow of reaction mixture (mL/min)	TOF (s^{-1})	Ref. no.
Au/SiO_2[a]	6	2	30	4.1×10^{-5}	[43]
$CeO_2\text{-}Au/SiO_2$[b]	6	2	30	0.103	[43]
$Au\text{-}CeO_2$[c]	14	1	50	0.080	[48]
Au/CeO_2 NP[d]	5.6	3	80	0.760	[21]
Au/CeO_2 NT[e]	3.8	3	80	0.950	[21]
Au/ZrO_2[f]	2.8	1	67	0.430	[84]
$Au@CeO_2$[g]	17	0.55	50	0.590	[48]
$Au@ZrO_2$[h]	14	6.8	67	0.206	[39]
$Au@ZrO_2$[h]	5.1	0.09	67	0.355	[42]
$Au@ZrO_2$[h]	14.7	4.87	67	0.254	[42]
$Au@ZrO_2$	15	0.55	80	0.463	This work
$Au\text{-}CeO_2@ZrO_2$	15	0.55	80	1.083	This work
$Au@SiO_2$	15	9.6	80	0.003	This work
$Au\text{-}CeO_2@SiO_2$	15	9.6	80	0.005	This work

[a] Au/SiO_2 (gold colloidal nanoparticles deposited on silica).
[b] $CeO_2\text{-}Au/SiO_2$ (gold colloidal nanoparticles deposited on silica and decorated by ceria (0.06 wt.%)).
[c] $Au\text{-}CeO_2$ (gold colloidal nanoparticles supported on CeO_2 sub-microspheres).
[d] Au/CeO_2 NP (gold nanoparticles formed from $Au(OH)_3$ deposited on ceria nanoparticles).
[e] Au/CeO_2 NT (gold nanoparticles formed from $Au(OH)_3$ deposited on ceria nanotubes).
[f] Au/ZrO_2 (colloidal gold nanoparticles covered with PVA and supported on ZrO_2. The presented TOF value corresponds to sample after decomposition of PVA at high temperature).
[g] $Au@CeO_2$ (gold nanoparticles encapsulated into porous CeO_2 shell).
[h] $Au@ZrO_2$ (gold nanoparticles encapsulated into porous ZrO_2 shell).

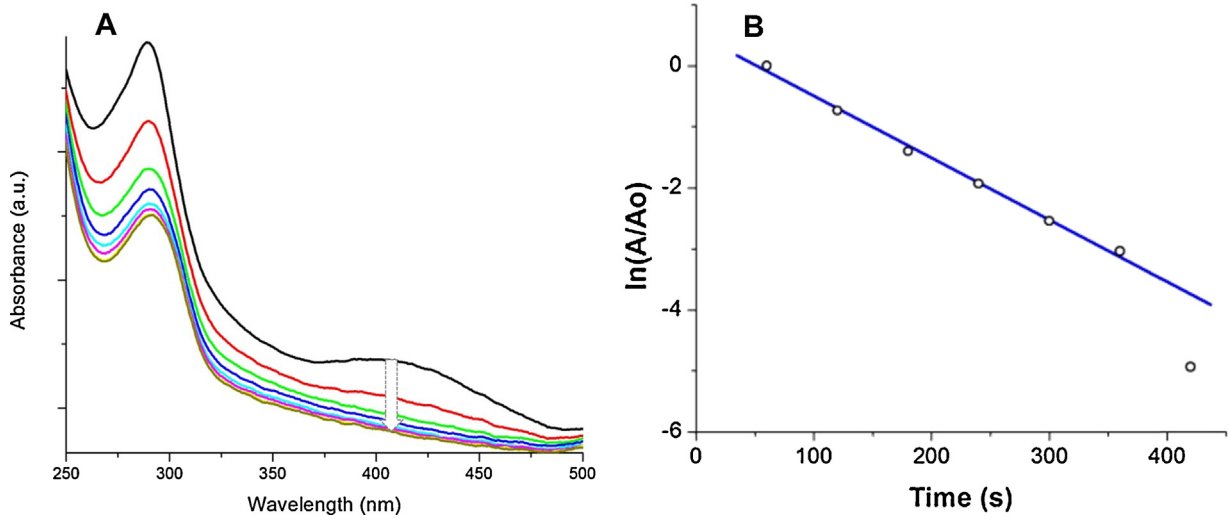

Fig. 8. Catalytic reduction of 2-nitrophenol by excess $NaBH_4$ in the presence of $Au\text{-}CeO_2@ZrO_2$ nanoreactors monitored by in situ UV–vis spectroscopy at room temperature (A). The change in absorbance at 415 nm corresponding to 2-nitrophenolate consumption in logarithmic form vs reaction time (B).

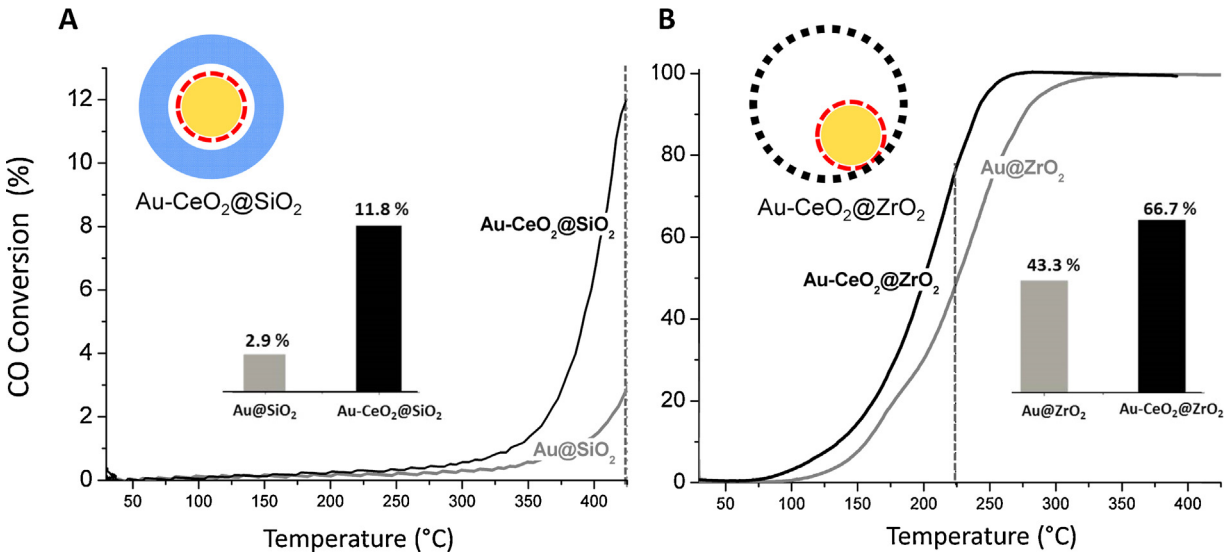

Fig. 9. Catalytic activity in CO oxidation of non-decorated and decorated nanoreactors encapsulated in silica (A) or in zirconia (B). Values displayed by bars correspond to CO conversion at the selected temperature marked by a dot line (insert).

plasmon band position neither for decorated nor for non-decorated nanoreactors (see Fig. 5). This implies that ceria did not noticeably affect the electronic state of Au cores. However, we cannot totally exclude the effect of a possible interaction of the surface defects in CeO_2 particles with the Au core, which can result in the formation of some portion of gold cations active in the 4-nitrophenol reduction [56]. On the other hand, the high efficiency of ceria to adsorb nitro aromatic molecules [57,58] can lead to an elevated local density of 4-nitrophenol and intermediate products of its partial reduction, and to the appearance of a second route for the 4-nitrophenol reduction via the condensation of these intermediates, with the resulting formation of 4-aminophenol. We suggest that the high affinity of ceria for the 4-nitrophenol adsorption strongly enhances the catalytic activity of the decorated nanoreactors. To confirm this suggestion, decorated and non-decorated nanoreactors were tested in the 2-nitrophenol to 2-aminophenol reduction. The 2-nitrophenol molecule is characterized by a strong intramolecular interaction between the hydroxyl group and the nitro group, which diminishes its capacity to be adsorbed on the oxide support surface, as compared with the 4-nitrophenol molecule [85]. Thus, in case of the reduction of 2-nitrophenol its high adsorption on ceria would not be expected. The characteristic peak at 415 nm for 2-nitrophenolate (Supplementary data Fig. S6) decreased with time of reaction (Fig. 8A). The value of the apparent reaction rate constants was estimated from a linear slope of the relative nitrophenolate ion content (A/A_o) in logarithmic form (see Fig. 8B). The decoration of nanoreactors with ceria apparently did not affect their catalytic performance in the 2-nitrophenol reduction (see Fig. 7). This confirms that affinity of ceria to adsorb 4-nitrophenol is crucial for the catalytic activity enhancement of the decorated nanoreactors in the reduction of 4-nitrophenol.

3.2.2. CO oxidation

It is well known that the Au/CeO_2 interface is much more active toward CO oxidation than gold in contact with silica [49]. Ceria participates in the reaction mechanism providing the activation of oxygen [86,87]. As expected, the decorated nanoreactors showed enhanced catalytic performance in comparison with the non-decorated nanoreactors (Fig. 9), which was attributed to the Au-ceria interface generated during the synthesis. In the case of the Au-CeO_2@SiO_2 nanoreactor, catalytic activity was improved by ~4 times compared with that for the non-decorated Au@SiO_2 nanoreactor. However, for Au-CeO_2@ZrO_2 nanoreactors the effect of the Ce decoration was less noticeable: activity was only enhanced by 1.5 times. This reduced improvement of Au-CeO_2@ZrO_2 nanoreactors in CO oxidation seems to be related with the partial decrease of the gold-ceria contact discussed above.

Data obtained for CO oxidation at 140 °C were compared with literature data for similar catalytic systems (see Table 2). CO oxidation strongly depends on the size of Au NPs, the nature of support/shell and the catalyst preparation method. As expected, the herein prepared Au@SiO_2 nanoreactors showed low activity as the Au NPs supported on silica [47]. However, the decoration of them with ceria (CeO_2-Au/SiO_2) resulted in more enhanced CO oxidation than that for the presently prepared Au-CeO_2@SiO_2 nanoreactor. Three factors may be used to explain this observation: (i) content of ceria near the Au NPs, (ii) size of the Au NPs, and (iii) mass transport limitation. Indeed, an estimate of the Au:CeO_2 molar ratio for the Au-CeO_2@SiO_2 gives a value three times lower than that for the CeO_2-Au/SiO_2. Note, that the size of the Au cores for the Au-CeO_2@SiO_2 is almost two times larger than that for the CeO_2-Au/SiO_2. For large Au NPs, the relative amount of gold atoms exposed to ceria (Au/CeO_2 interface active in CO oxidation) is lower than for small Au NPs. In addition, the silica shell of the Au-CeO_2@SiO_2 is rather thick (26 nm), and this can cause mass transport problems.

On the other hand, the zirconia shell is rather thin (11 nm, see Fig. S4 in Supplementary data), which cannot lead to significant mass transfer problems [39]. CO oxidation activity of the herein prepared Au@ZrO_2 nanoreactor was slightly higher than that of the reference nanoreactors and almost equal to that shown by supported Au/ZrO_2 catalysts (see Table 2) [39,42,88]. In contrary with supported catalysts, the zirconia shell of nanoreactors prepared via silica template commonly includes some amounts of a residual silica. It was suggested that the zirconia shell in the herein prepared Au@ZrO_2 nanoreactor contains lower amounts of silica than reference nanoreactors. A similar suggestion was made for the reaction of the 4-nitrophenol reduction over the same nanoreactors. As expected, introduction of ceria into the void space of the Au@ZrO_2 nanoreactors resulted in a noticeable activity increase. The effect of ceria on CO oxidation over Au catalysts strongly depends on the preparation methods. Colloidal Au NPs deposited on ceria nanospheres (Au-CeO_2) are characterized by weak Au-ceria interaction and low catalytic activity [48], in

contrast, Au NPs formed via decomposition of $Au(OH)_3$ pre-supported on either ceria nanoparticles (Au/CeO_2 NP) or nanotubes (Au/CeO_2 NT) present high activity [21]. Note that the TOF values for the herein prepared Au-CeO_2@ZrO_2 nanoreactors and the Au/CeO_2 NT supported catalysts were comparable.

4. Conclusions

Highly catalytically active Au-CeO_2@ZrO_2 nanoreactors for the 4-nitrophenol to 4-aminophenol reduction were synthesized by decoration of the gold cores with ceria species in yolk–shell Au@ZrO_2 nanoreactors. The proposed route allows the decoration of Au cores with ceria by forming ceria species in the void space of the nanoreactor via homogeneous hydrolysis of ceria precursor in the presence of urea. The creation of the gold-ceria interface in decorated nanoreactors was confirmed by the presence of both elements near the core, changes in the gold electronic state and enhanced catalytic activity in the 4-nitrophenol reduction to 4-aminophenol and CO oxidation. The proposed route may be applied to the synthesis of nanoreactors containing Au cores modified with different materials in order to make them effective for diverse catalytic reactions.

Acknowledgements

The authors thank O. Callejas, J. Mendoza, E. Flores, F. Ruiz, J. Peralta and M. Sainz for technical assistance and M.I. Perez Montfort for revising the English version of the manuscript. This research project was partially supported by CONACyT (México) and PAPIIT-UNAM (México) through Grants 179619 and 203813, respectively.

Appendix A. Supplementary data

Supplementary data associated with this article can be found, in the online version, at http://dx.doi.org/10.1016/j.apcatb.2014.12.006.

References

[1] M. Haruta, T. Kobayashi, H. Sano, N. Yamada, Chem. Lett. 16 (1987) 405.
[2] K. Kuroda, T. Ishida, M. Haruta, J. Mol. Catal. A: Chem. 298 (2009) 7–11.
[3] S. Wunder, F. Polzer, Y. Lu, Y. Mei, M. Ballauff, J. Phys. Chem. C 114 (2010) 8814–8820.
[4] M. Haruta, J. New Mater. Electrochem. Syst. 7 (2004) 163–172.
[5] C. Yang, M. Kalwei, F. Schüth, K. Chao, Appl. Catal. A: Gen. 254 (2003) 289–296.
[6] V. Idakiev, T. Tabakova, Z.-Y. Yuan, B.-L. Su, Appl. Catal. A: Gen. 270 (2004) 135–214.
[7] Q. Fu, S. Kudriavtseva, H. Saltsburg, M. Flytzani-Stephanopoulos, Chem. Eng. J. 93 (2003) 41–53.
[8] A. Corma, H. Garcia, Chem. Soc. Rev. 37 (2008) 2096–2126.
[9] J.A. Lopez-Sanchez, N. Dimitritos, C. Hammond, G.L. Brett, L. Kesavan, S. White, P. Miedziak, R. Tiruvalam, R.L. Jenkins, A.F. Carley, D. Knight, C.J. Kiely, G.J. Hutchings, Nat. Chem. 3 (2011) 551.
[10] P. Forzatti, L. Lietti, Catal. Today 52 (1999) 165–181.
[11] C.H. Bartholomew, Appl. Catal. A: Gen. 212 (2001) 17–60.
[12] N. Mandzy, E. Grulke, T. Druffel, Powder Technol. 160 (2005) 121–126.
[13] D.H. Napper, A. Netschey, J. Colloid Interface Sci. 37 (1971) 528–535.
[14] N.M. Wichner, J. Beckers, G. Rothenberg, H. Koller, J. Mater. Chem. 20 (2010) 3840–3847.
[15] J. Zhu, Z. Konya, V.F. Puntes, I. Kiricsi, C.X. Miao, J.W. Ager, A.P. Alivisatos, G.A. Somorjai, Langmuir 19 (2003) 4396–4401.
[16] I. Tuzovskaya, N. Bogdanchikova, A. Simakov, V. Gurin, A. Pestryakov, M. Avalos, M.H. Farias, Chem. Phys. 338 (2007) 23–32.
[17] A. Simakov, I. Tuzovskaya, A. Pestryakov, N. Bogdanchiva, V. Gurin, M. Avalos, M.H. Farias, Appl. Catal. A: Gen. 331 (2007) 121–128.
[18] X. Huang, C. Guo, J. Zuo, N. Zheng, G.D. Stucky, Small 5 (3) (2009) 361–365.
[19] R.G. Chaudhuri, S. Paria, Chem. Rev. 112 (2012) 2373–2433.
[20] R. Zanella, V. Rodríguez-González, Y. Arzola, A. Moreno-Rodríguez, ACS Catal. 2 (2012) 1–11.
[21] B. Acosta, E. Smolentseva, S. Beloshapkin, R. Rangel, M. Estrada, S. Fuentes, A. Simakov, Appl. Catal. A: Gen. 449 (2012) 96–104.
[22] A. Sandoval, A. Aguilar, C. Louis, A. Traverse, R. Zanella, J. Catal. 281 (2011) 40–49.
[23] P.M. Arnal, M. Comotti, F. Schuth, Angew. Chem. Int. Ed. 45 (2006) 8224–8227.
[24] Q. Zhang, I. Lee, J. Ge, F. Zaera, Y. Yin, Adv. Funct. Mater. 20 (2010) 2201–2214.
[25] I. Lee, M. Albiter, Q. Zhang, J. Ge, Y. Yin, F. Zaera, Phys. Chem. Chem. Phys. 13 (2011) 2449–2456.
[26] X.W. Lou, L.A. Archer, Z. Yang, Adv. Mater. 20 (2008) 3987–4019.
[27] J.C. Park, H. Song, Nano Res. 4 (1) (2011) 33–49.
[28] L. Kong, G. Duan, G. Zuo, W. Cai, Z. Cheng, Mater. Chem. Phys. 123 (2010) 421–426.
[29] J. Ge, Q. Zhang, T. Zhang, Y. Yin, Angew. Chem. Int. Ed. 47 (2008) 8924–8928.
[30] J. Lee, J.C. Park, H. Song, Adv. Mater. 20 (2008) 1523–1528.
[31] M. Cargnello, N.L. Wieder, T. Montini, R.J. Gorte, P. Fornasiero, J. Am. Chem. Soc. 132 (2010) 1402–1409.
[32] A. Dangwal, R. Güttel, M. Leoni, F. Schüth, C. Weidenthaler, J. Phys. Chem. C 114 (2010) 19386–19394.
[33] H. Yin, Z. Ma, M. Chi, S. Dai, Catal. Today 160 (2011) 87–95.
[34] R. Güttel, M. Paul, F. Schüth, Chem. Commun. 46 (2010) 895–897.
[35] G. Li, Z. Tang, Nanoscale 6 (2014) 3995–4011.
[36] Y. Zhao, L. Jiang, Adv. Mater. 21 (2009) 1–18.
[37] J. Liu, S.Z. Quiao, J.S. Chen, X.W. (David) Lou, X. Xing, G.Q. (Max) Lu, Chem. Commun. 47 (2011) 12578–12591.
[38] P. Arnal, C. Weidenthaler, F. Schuth, Chem. Mater. 18 (2006) 2733–2739.
[39] C. Galeano, R. Guttel, M. Paul, P. Arnal, A. Lu, F. Schuth, Chem. – Eur. J. 17 (2011) 8434–8439.
[40] M. Haruta, Catal. Today 36 (1997) 153–166.
[41] M. Haruta, N. Yamada, T. Kobayashi, S. Iijima, J. Catal. 115 (1989) 301–309.
[42] R. Güttel, M. Paul, C. Galeano, F. Schüth, J. Catal. 289 (2012) 100–104.
[43] A. Samanta, T. Rajesh, R.N. Devi, J. Mater. Chem. A 2 (2014) 4398–4405.
[44] C. Chen, M. Shi, M. Cargnello, P. Fornasiero, C.B. Murray, R.J. Gorte, Catal. Lett. 144 (2014) 1939–1945.
[45] Q. Zhang, T. Zhang, J. Ge, Y. Yin, Nano Lett. 8–9 (2008) 2867–2871.
[46] X. Fang, Z. Liu, M.-F. Hsieh, M. Chen, P. Liu, C. Chen, N. Zheng, ACS Nano 6 (5) (2012) 4434–4444.
[47] A. Horvath, A. Beck, G. Stefler, T. Benko, G. Safran, Z. Varga, J. Gubicza, L. Guczi, J. Phys. Chem. C 115 (2011) 20388–20398.
[48] Z. Zhou, M. Flytzani-Stephanopoulos, H. Saltsburg, J. Catal. 280 (2011) 255–263.
[49] Z. Zhou, S. Kooi, M. Flytzani-Stephanopoulos, H. Saltsburg, Adv. Funct. Mater. 18 (2008) 2801–2807.
[50] R. Guttel, M. Paul, F. Schüth, Catal. Sci. Technol. 1 (2011) 65–68.
[51] M. Cargnello, C. Gentilini, T. Montini, E. Fonda, S. Mehraeen, M. Chi, M. Herrera-Collado, N.D. Browning, S. Polizzi, L. Pasquato, P. Fornasiero, Chem. Mater. 22 (2010) 4335–4345.
[52] J. Qi, J. Chen, G. Li, S. Li, Y. Gao, Z. Tang, Energy Environ. Sci. 5 (2012) 8937–8941.
[53] C. Fan, L. Zhang, S. Wang, D. Wang, L. Lu, A. Xu, Nanoscale 4 (2012) 6835–6840.
[54] B. Liu, S. Yu, Q. Wang, W. Hu, P. Jing, Y. Liu, W. Jia, Y. Liu, L. Liu, J. Zhang, Chem. Commun. 49 (2013) 3757–3759.
[55] H.-Z. Zhu, Y.-M. Lu, F.-J. Fan, S.-H. Yu, Nanoscale 5 (2013) 7219–7223.
[56] J. Zhang, G. Chen, M. Chaker, F. Rosei, D. Ma, Appl. Catal. B: Environ. 132–133 (2013) 107–115.
[57] D. Combita, P. Concepcion, A. Corma, J. Catal. 311 (2014) 339–349.
[58] M. Makosch, J. Sa, C. Kartusch, G. Richner, J.A. van Bokhoven, K. Hungerbuhler, ChemCatChem 4 (2012) 59–63.
[59] J. Turkevich, P. Stevenson, J. Hillier, J. Phys. Chem. 57 (7) (1953) 670–673.
[60] J. Kimling, M. Maier, B. Okenve, V. Kotaidis, H. Ballot, A. Plech, J. Phys. Chem. B 110 (2006) 15700–15707.
[61] W. Stöber, A. Fink, E. Bohn, J. Colloid Interface Sci. 26 (1968) 62–69.
[62] K. Nozawa, H. Gailhanou, L. Raison, P. Panizza, H. Ushiki, E. Sellier, J.P. Delville, M.H. Delville, Langmuir 21 (2005) 1516–1523.
[63] Y. Hu, Q. Zhang, J. Goebl, T. Zhang, Y. Yin, Phys. Chem. Chem. Phys. 12 (2010) 11836–11842.
[64] Q. Zhang, T. Zhang, J. Ge, Y. Yin, Nano Lett. 8 (9) (2008) 2867–2871.
[65] Q. Zhang, J. Ge, J. Goebl, Y. Hu, Z. Lu, Y. Yin, Nano Res. 2 (2009) 583–591.
[66] Q. Zhang, W. Wang, J. Goebl, Y. Yin, Nano Today 4 (2009) 494–507.
[67] L. Carbone, P. Cozzoli, Nano Today 5 (2010) 449–493.
[68] Z. Wang, D. Luan, C. Ming Li, F. Su, S. Madhavi, F. Yin Chiang Boey, X. Wen Lou, J. Am. Chem. Soc. 132 (2010) 16271–16277.
[69] M. Hirano, M. Inagaki, J. Mater. Chem. 10 (2000) 473–477.
[70] D.L. Feldheim, C.A. Foss, Metal Nanoparticles: Synthesis, Characterization and Applications, Marcel Dekker Inc., Basel, New York, 2002.
[71] E. Smolentseva, B.T. Kusema, S. Beloshapkin, M. Estrada, E. Vargas, D. Yu Murzin, F. Castillon, S. Fuentes, A. Simakov, Appl. Catal. A: Gen. 392 (2011) 69–79.
[72] A.I.Y. Tok, F.Y.C. Boey, Z. Dong, X.L. Sun, J. Mater. Process. Technol. 190 (2007) 217–222.
[73] G. Perez, S. Fuentes, V. Petranovskii, A. Simakov, Catal. Lett. 110 (2006) 53–60.
[74] E. Smolentseva, A. Simakov, S. Beloshapkin, M. Estrada, E. Vargas, V. Sobolev, R. Kenzhin, S. Fuentes, Appl. Catal. B: Environ. 115–116 (2012) 117–128.
[75] M. Boronat, P. Concepción, A. Corma, S. González, F. Illas, P. Serna, J. Am. Chem. Soc. 129 (2007) 16230–16237.
[76] K. Shimizu, Y. Miyamoto, T. Kawasaki, T. Tanji, Y. Tai, A. Satsuma, J. Phys. Chem. C 113 (2009) 17803–17810.
[77] H. Liu, Q. Yang, J. Mater. Chem. 21 (2011) 11961–11967.
[78] S. Nuretti, O. Ozgur, Curr. Nanosci. 8 (2012) 367–374.
[79] K.S. Shin, Y.K. Cho, J.-Y. Choi, K. Kim, Appl. Catal. A: Gen. 413–414 (2012) 170–175.
[80] S.M. El-Sheikh, A. Ismail, J. Al-Shara, New J. Chem. 37 (2013) 2399–2407.
[81] P. Herves, M. Perez-Lorenzo, L.M. Liz-Marzan, J. Dzubiella, Y. Lu, M. Ballauff, Chem. Soc. Rev. 41 (2012) 5577–5587.

[82] C. Yang-Chuang, C. Dong-Hwang, J. Hazard. Mater. 165 (2009) 664–669.
[83] P. Veerakumar, M. Velayudham, K. Lu, S. Rajagopala, Appl. Catal. A: Gen. 439–440 (2012) 197–205.
[84] J. Li, C. Liu, Y. Liu, J. Mater. Chem. 22 (2012) 8426–8430.
[85] A. Feigenbaum, J. Chem. Educ. 63–69 (1986) 815–817.
[86] J. Guzman, S. Carrettin, A. Corma, J. Am. Chem. Soc. 127 (2005) 3286–3287.
[87] S. Carrettin, P. Concepcion, A. Corma, J.M. Lopez-Nieto, V.F. Puntes, Angew. Chem. Int. Ed. 43 (2004) 2538–2540.
[88] M. Comotti, W.-C. Li, B. Sliethoff, F. Schüth, J. Am. Chem. Soc. 128 (2006) 917–924.